Heat Conductivity of Amorphous Solids: Simulation Results on Model Structures

Ping Sheng; Minyao Zhou

Science, New Series, Vol. 253, No. 5019. (Aug. 2, 1991), pp. 539-542.

Stable URL:
http://links.jstor.org/sici?sici=0036-8075%2819910802%293%3A253%3A5019%3C539%3AHCOASS%3E2.0.CO%3B2-X

Science is currently published by American Association for the Advancement of Science.

Reports

Heat Conductivity of Amorphous Solids: Simulation Results on Model Structures

PING SHENG AND MINYAO ZHOU

Through numerical simulation and consideration of phonon scattering by two-level states, the heat conductivity $\kappa(T)$, where T is temperature, has been calculated on model structures. The values obtained are in good quantitative agreement with measured data on polymethylmethacrylate, epoxy, amorphous selenium, and amorphous silicon dioxide over the temperature range 0.1 to 100 K. The calculated results reproduce the plateau feature, in the range of 5 to 20 K, that is generic to the heat conductivity of amorphous solids. Two model parameters, one characterizing the degree of structural disorder and the other related to the relaxational absorption of two-level states, are identified as being responsible for the behavior of $\kappa(T)$ at $T \geq 5$ K. The simulation results indicate the existence of a frequency-independent phonon diffusion regime that is consistent with the minimum phonon mean-free-path hypothesis. The magnitude of the phonon diffusion constant in this regime is shown to give a reasonable quantitative account of high-temperature $\kappa(T)$ in amorphous systems.

THE INTRIGUING DIFFERENCES IN the heat conductivity of amorphous and crystalline solids have been a topic of continued study and debate for the past four decades. At temperatures $\lesssim 1$ K, amorphous solids display a quadratic temperature dependence (*1*) instead of the T^3 dependence exhibited by insulating crystals. This behavior is well understood in terms of the two-level (T-L) states theory (*2–4*), although the physical basis of the T-L states has not yet been individually identified for every amorphous system. A second difference, which is the focus of this study, is the existence of a "plateau" region in the heat conductivity (*5*) of amorphous solids, usually extending from 5 to 30 K, that is always followed by a further rise at higher temperatures. Various theories interpret the plateau (*6–9*) and its subsequent rise (*10–15*) as resulting from phonon localization, phonon-fracton crossover, the existence of a minimum phonon mean free path, hopping transport, and so on. However, there is still a lack of consistent demonstration of the plateau phenomenon, including its subsequent rise, from a given structural model. A demonstration of this phenomenon would be valuable not only in identifying the possible mechanism or mechanisms leading to the thermal conductivity plateau but would also test the degree to which the distinct features of the heat conductivity of amorphous solids are the generic and universal consequences of disordered structures.

We report here the results of numerical simulation on a model amorphous system. By combining our simulation results with the T-L states theory, we demonstrate that not only can the plateau feature be reproduced, but the calculated heat conductivity is also in good quantitative agreement with experimental data on four different amorphous solids. Two physical parameters, plus the existence of an unusual phonon diffusion regime, are identified as being key to the plateau phenomenon and its subsequent high-temperature saturation.

Because the phenomenon we address is generic to a wide class of amorphous solids, the element of structural disorder, which is a common feature of all amorphous materials, should be incorporated in any model. It also follows that features specific to each material, such as chemical composition, chemical bonding, local structural order, the type of disorder, and so forth, should be less important to the plateau phenomenon. On the basis of these considerations, we chose as our structure the simple model of a percolation network, obtained by randomly placing atoms on a fraction p of the simple cubic lattice sites and then removing the isolated clusters. Here p is a parameter that controls the amount of disorder. The requirement that the structure be connected means that p must be greater than the percolation threshold (*16*) $p_c \simeq 0.31$. By construction, the number density of the percolation network is less than p. However, as long as $p > 0.5$, the difference between the actual density and p is small and will therefore be neglected. Because at $p > 0.5$ the percolation network is far from the percolation threshold, the structure is always compact and fractal structure effect is not a consideration. At temperatures lower than the plateau regime, the heat conductivity of amorphous solids is dominated by phonon scattering by T-L states; therefore, we also assume that our model structure is decorated by a given density of T-L states.

The heat conductivity $\kappa(T)$, where T denotes temperature, can be written as

$$\kappa(T) = \int_0^\infty n(\omega)\, C\left(\frac{\hbar\omega}{kT}\right) D(\omega)\, d\omega \qquad (1)$$

where ω is frequency, k is the Boltzmann constant, $\hbar$ is Planck's constant, $n(\omega)$ denotes phonon density of states, $D(\omega)$ is the phonon diffusion constant, and C is the specific heat of a phonon mode, given by

$$C(x) = k\, x^2 \frac{\exp(x)}{[\exp(x) - 1]^2} \qquad (2)$$

Here $x = \hbar\omega/kT$. In our model, $D(\omega)$ has two contributions: diffusion due to scattering from random geometry, denoted $D_R(\omega)$, and diffusion due to scattering from two-level states, denoted as $D_{TL}(\omega)$. Because these two types of scattering are parallel processes, under the assumption of additivity of rates they are related to the overall diffusion constant $D(\omega)$ by

$$D(\omega) = [D_R^{-1}(\omega) + D_{TL}^{-1}(\omega)]^{-1} \qquad (3)$$

where $D_{TL}(\omega)$ is known to be in the form (*1, 8*) of

$$D_{TL}^{-1}(\omega) = A\left(\frac{\hbar\omega}{k}\right) \tanh\left(\frac{2\hbar\omega}{kT}\right) + \frac{A}{2}\left[\frac{BT^3}{1 + \left(\frac{kT}{\hbar\omega}\right)BT^2}\right] \qquad (4)$$

The first term of Eq. 4 is due to resonant scattering, whereas the second term is due to relaxational absorption. The constant A is proportional to the product of T-L state density and the square of the phonon–T-L state coupling constant. Its value is fixed by the slope of the T^2 variation at temperatures below the plateau regime. That means p and B are the only two adjustable parameters for the plateau phenomenon in our model.

Consider the scalar displacement field ϕ on a 79 by 79 by 79 percolating network that satisfies the equation

$$m\frac{d^2\phi_i}{dt^2} = \sum_j \beta_{ij}(\phi_j - \phi_i) \qquad (5)$$

where i,j are the site indices that only count

Exxon Research and Engineering Company, Route 22 East, Annandale, NJ 08801.

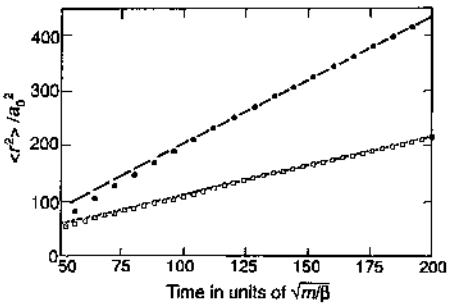

Fig. 1. Variation of mean square distance with time for $p = 0.65$ and two different frequencies, $\omega = \sqrt{\beta/m}/2$ (□) and $\omega = \pi\sqrt{\beta/m}/4$ (●). The dashed line indicate the asymptotic linear behavior of $<r^2>$ as a function of time.

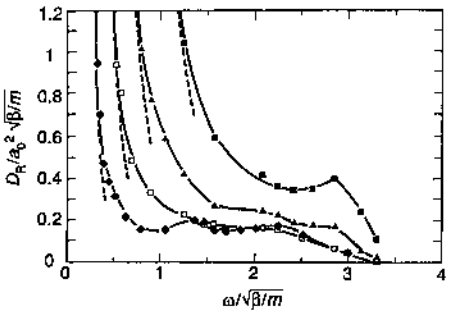

Fig. 2. Variation of the diffusion constant D_R with frequency for four values of p: 0.85 (■), 0.75 (▲), 0.65 (□), and 0.55 (◆). The dashed lines denote the ω^{-4} asymptotic variation due to Rayleigh scattering.

occupied sites, m denotes the atomic mass, $\beta_{ij} = \beta$ if sites i and j are nearest neighbors, and $\beta_{ij} = 0$ otherwise. Equation 5 is the discrete version of the scalar wave equation, $\partial^2\phi/\partial t^2 - c^2\nabla^2\phi = 0$, where $c = a_0\sqrt{\beta/m}$, a_0 being the lattice constant. Although the phonon field is recognized as vector in nature, the scalar model is still expected to capture the essential features of $\kappa(T)$, which represents an integral effect of many phonons, in much the same spirit as the Debye model of specific heat.

In order to obtain values of D_R on the percolation network, an excitation of frequency ω, modulated with a Gaussian envelope of half-width $\Delta t = 6\pi/\omega$ to $18\pi/\omega$, is imposed on a single site close to the center of the network. The width of the source pulse implies a frequency spectrum width of about 0.1 to 0.3 times ω. One can calculate the subsequent spread of the pulse numerically on a Cray-XMP computer by using Eq. 5 up to the time when the pulse peak hits the sample boundary. The mean square radius $<r^2(t)>$ is calculated as

$$<r^2(t)> = \frac{\sum_i \phi_i^2(t)\, r_i^2}{\sum_i \phi_i^2(t)} \qquad (6)$$

where r_i is the distance between site i and the excitation site, and the averaging is done by using the intensity ϕ_i^2 of the phonon at site i (which is proportional to the local energy density) as the weight. A similar space-time simulation technique has been used to calculate the diffusion constant of electrons (*17*). Figure 1 shows $<r^2(t)>$, in units of (lattice constant a_0)^2, as a function of time, in units of $\sqrt{m/\beta}$. The value of p is 0.65. Results for two frequencies, $\omega/\sqrt{\beta/m} = \pi/2$ and $\omega/\sqrt{\beta/m} = \pi/4$, are displayed. Excellent asymptotic linear variation is seen; thus $D_R(\omega)$ may be evaluated as one-sixth of the asymptotic slopes. A single configuration can yield accurate results, and the value of $D_R(\omega)$ has been checked to be repeatable from one configuration to the next (*18*), provided p stays the same and is ≥ 0.5.

For $p = 0.75$, 0.65, and 0.55, the $D_R(\omega)$ values thus calculated are plotted in Fig. 2. Because we use a pulse excitation in our simulation, the frequency value of each point in the figure should be interpreted as the mean value averaged over a frequency window of $\omega \pm 0.1\omega$. Variation in the pulse width was found to have an insignificant effect on our results. At low frequencies, $D_R(\omega)$ is seen to always approach the ω^{-4} dependence (indicated by the dashed line) dictated by Rayleigh scattering. At the frequency $\omega = \omega_c$ where the mean free path $\ell = 3D_R(\omega)/v$, where v denotes the acoustic velocity, is on the order of the mean separation between scatterers, $D_R(\omega)$ levels off to a plateau value, and for $p < 0.65$ the plateau value seems to stay constant at $D_0 = 0.17\, a_0^2\sqrt{\beta/m}$.

This behavior supports the minimum mean-free-path hypothesis (*8–14*), but, because the dispersion relation is not linear in this frequency range so that the phonon velocity is not well defined, conversion from diffusion constant to mean free path would have dubious meaning. Nevertheless, an explanation based on the minimum mean-free-path idea could be formulated for this diffusion regime (see below). At frequencies close to the band edge (*19*) ($=\sqrt{12\beta/m}$ for $p = 1$), the linear $<r^2(t)>$ versus t asymptotic behavior is modified into a saturation behavior, implying $D_R(\omega) \approx 0$. This is a reflection of phonon localization, which is known to occur first at the phonon band edge (*20*) as the amount of disorder is increased.

For the phonon density of states $n(\omega)$, we use the recursive Green's function technique (*21*) to evaluate the local density of states $n_0(\omega)$ numerically. The phonon density of states is then obtained as the configurational average of $3n_0(\omega)$, where the factor 3 accounts for each atom's three degrees of freedom. Figure 3A compares our numerical calculation for $n(\omega)$, normalized to each atom, with the known exact result for $p = 1$. (No configurational average is necessary here because every site is equivalent in this case.) At low frequencies, $a^3n(\omega) = \omega^2a^3(2\pi^2v^3)^{-1}$, where $a^3 = a_0^3/p$ is the atomic volume, and $v = a_0\sqrt{\beta/m}$ is the acoustic velocity (dashed line in Fig. 3A). In Fig. 3B we show the calculated $n(\omega)$ for $p = 0.55$, obtained by averaging over 100 configurations, each 79 by 79 by 79. At low frequencies the acoustic velocity $v = (\beta_{eff}/m_{eff})^{1/2}$, where $m_{eff} = pm$ and β_{eff} = (probability that nearest-neighbor sites i and j are both occupied) $\times\ \beta = p^2\beta$. Therefore,

$$v = \sqrt{p}\sqrt{\frac{\beta}{m}}\,a_0 \qquad (7)$$

By using this v we get an excellent fit to the low-frequency $n(\omega)$ (dashed line in Fig. 3B), which delineates the density of states for the Debye model.

By using the simulated $D_R(\omega)$ and $n(\omega)$, we can evaluate the heat conductivity $\kappa(T)$ by numerical integration of Eq. 1. To convert our results into actual physical units, the

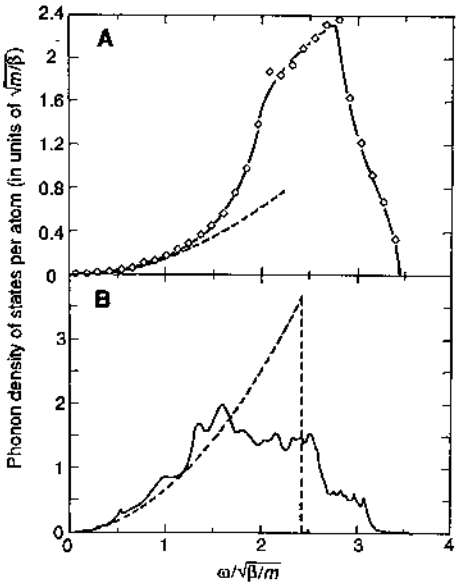

Fig. 3. (**A**) Phonon density of states for the perfect lattice, $p = 1$, normalized to each atom. Open diamonds denote the exact solution. The solid line denotes the numerical results that one would obtain by using the recursive Green's function method. The dashed line denotes the low-frequency behavior of the Debye model. (**B**) Phonon density of states for the percolation cluster at $p = 0.55$, normalized to each atom. The solid line denotes the numerical result obtained by using the recursive Green's function approach. The dashed line denotes the Debye model. Compared with (A), there is in (B) a significant shift downward in the density of states due to the softening of the lattice and the decrease of the acoustic velocity.

magnitudes of a_0 and $\sqrt{\beta/m}$ are needed. For this conversion, we equate the average atomic volume a^3 to a_0^3/p, that is, $a_0 = p^{1/3}a$, and use Eq. 7 to get $\sqrt{\beta/m}$, or $\sqrt{\beta/m} = v/(\sqrt{p}\, a_0) = p^{-5/6}v/a$, where we use the measured acoustic velocity of the material for v. Figure 4 shows the results obtained for the $\kappa(T)$ of four materials (*8*) (we have used $p = 0.55$ in all four cases). The material parameters used are $v = 1.79 \times 10^5$ cm s^{-1} and $a = 2.86$ Å for polymethylmethacrylate (PMMA) (*8, 22*); $v = 1.66 \times 10^5$ cm s^{-1} and $a = 2.9$ Å for epoxy (*8, 23*); $v = 1.56 \times 10^5$ cm s^{-1} and $a = 3.12$ Å (calculated from a density of 4.3 g/cm^3 and atomic number of 79) for amorphous Se (*8*); and $v = 4.1 \times 10^5$ cm s^{-1} and $a = 2.47$ Å for amorphous SiO_2 (*8, 22*). For the value of A, we used the literature values (*8*) of 2.63×10^{-3} s^{-1} K^{-1} for amorphous SiO_2, 2.22×10^{-2} s^{-1} K^{-1} for amorphous Se, 1.68×10^{-2} s^{-1} K^{-1} for PMMA, and 2.08×10^{-2} s^{-1} K^{-1} for epoxy. The values of B obtained from the fits are 26.5×10^{-3} K^{-2}, 12.3×10^{-3} K^{-2}, 21.6×10^{-3} K^{-2}, and 38×10^{-3} K^{-2} for PMMA, epoxy, amorphous Se, and amorphous SiO_2, respectively. The B values for PMMA and amorphous SiO_2 do exhibit significant differences from those obtained by Graebner *et al.* (*8*), whereas those for epoxy and amorphous Se are close. Lack of experimental data on the value of B precludes a judgment as to the reasonableness of our fitted values.

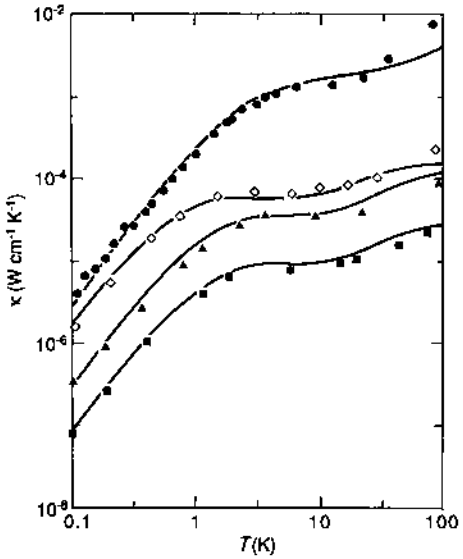

Fig. 4. Log-log plot of heat conductivity κ versus temperature T. Symbols denote a subset of data taken from (*8*), displaced from each other for clarity. Epoxy data (■) are divided by 64. PMMA data (▲) are divided by 16. Amorphous Se data (◇) are divided by 8. Amorphous SiO_2 data are denoted by (●). Solid lines show the calculated results. Values of the parameters used are given in the text.

Three points about Fig. 4 should be noted. First, the magnitude of calculated $\kappa(T)$ is in good overall agreement with the experimental data, even though we did not attempt to fine-tune the fitting by adjusting p. Second, in our calculation p controls the absolute value of $\kappa(T)$ for $T > 5$ K as well as the plateau width; that is, as p increases, the plateau region shrinks in width and increases in magnitude until above $p = 0.85$ the plateau completely disappears. The parameter B, on the other hand, controls only the slope of the plateau. The rise in $\kappa(T)$ beyond the plateau is virtually independent of the T-L states and is dependent only on D_0 and the density of states. This dependence may be made quantitative as seen later. Third, our fits are insensitive to changes of p and B. The value of p may be varied by a few percent and B may be adjusted upward or downward by 10 or 20% without significantly degrading the quality of agreement.

Within the framework of our model, the origin of the plateau phenomenon may be described as follows. From the simulated results for $p = 0.55$ the product $n(\omega)D(\omega)$ has a valley at approximately $\omega/\sqrt{\beta/m} \approx 1$. As $n(\omega)D(\omega)$ is integrated with $C(\hbar\omega/kT)$ with $B = 0$, that is, no relaxational absorption, the result is a monotonically increasing $\kappa(T)$ in which there is an inflection point, namely, a temperature region of slow increase (due to the Rayleigh scattering), followed by a faster rise [due to the rising $n(\omega)D(\omega)$] of $\kappa(T)$. The role of B, which from Eq. 4 is seen to control the relaxational absorption of T-L states, is simply to add a temperature-dependent component to $D(\omega)$ which decreases $D(\omega)$ as T increases, thus accentuating the inflection point in $\kappa(T)$ into a plateau. Therefore, in our model the plateau is due to Rayleigh scattering, but the rise after the plateau and the eventual saturation of $\kappa(T)$ are due to the constant $D_R(\omega)$ [so that the $n(\omega)$ peak is reserved in the product $n(\omega)D(\omega)$] and the eventual localization of phonons.

The existence of a constant $D_R(\omega) \simeq D_0$ region is crucial to the behavior of $\kappa(T)$ for $T \gtrsim 10$ K. A possible explanation for this unusual region of $D_R(\omega)$ is as follows. As frequency increases in the Rayleigh scattering regime, the rapidly increasing scattering strength would sharply decrease the mean free path ℓ to $\bar{\ell}$ at $\omega \simeq \omega_{\ell}$, where $\bar{\ell}$ is the mean separation between scattering centers. Beyond that point, both v and wave vector $\mathbf{k}$ can no longer meaningfully characterize the phonon states due to the strong scattering, and the phonon eigenfunctions are expected to become inhomogeneous on the scale of $\bar{\ell}$ and disordered spatially. However, the phonons in this regime are still not localized because they display a finite diffusion constant.

Because our simulation is done on a finite sample, the localized state that is most difficult to detect is one in which the localization length diverges, that is, the state at the mobility edge, However, localization theory predicts that the diffusion constant of such a "nearly localized" state is inversely proportional to the diffused distance so that instead of $\langle r^2 \rangle \propto$ time, one would obtain $\langle r^3 \rangle \propto$ time (*24*). In other words, there is finite-time manifestation of a localized state, even if the localization length is infinite. In Fig. 1, the line with open squares is representative of the time evolution behavior for a frequency point in the regime under discussion. Clearly, no $\langle r^3 \rangle \propto$ time type of characteristic is seen, indicating that the state is not even "nearly localized." The fact that we do see localization near the band edge is further proof that it is not that we cannot detect localization, but that the states in this unusual regime are actually not localized.

For the diffusion constant in this regime, if one writes $D_R \propto \bar{\ell}^2/\tau$, then τ is given by the only intrinsic time scale in the problem, $\bar{\ell}^3 n(\omega)$. This τ repesents the inverse of the mean frequency separation between phonon eigenstates in a volume $\bar{\ell}^3$, and it governs the time evolution of any state that is a linear superposition of the inhomogeneous eigenfunctions. The overall physical picture of this regime thus bears resemblance to that proposed by Einstein (*11*). However, whereas in the Einstein model and its later generalization (*12–14*) the diffusion constant is either proportional or inversely proportional to ω, here it is an approximate constant. This diffusive regime would persist until the phonon localization effect sets in near the band edge.

The relation between the (nearly) constant value of $D_R(\omega) = D_0$ and the high-temperature saturation value of $\kappa(T)$, κ_s, can be isolated and made quantitative. That is, if we focus on the quantity $\Delta\kappa = \kappa_s - \kappa(10\text{ K})$, then $\Delta\kappa$ is virtually independent of the T-L states characteristics and is controlled only by D_0 and $n(\omega)$. In our model, one can calculate $\Delta\kappa$ from Eq. 1 by replacing the lower bound of the integral by ω_{ℓ} and setting $T \to \infty$ and $D(\omega) = D_R(\omega)$. That yields $\Delta\kappa = K_0 v k/a^2$, where $K_0 = 0.49$ for $p = 0.55$ is a dimensionless constant. If we approximate κ_s by $\kappa(300\text{ K})$, then experimentally $K_0 = 0.35$, 0.45, 0.59, 1.2, 0.62, and 0.28 for epoxy, PMMA, amorphous Se, amorphous SiO_2, nitrate glass (*13*), and As_2S_3 (*13*), respectively. Apart from amorphous SiO_2 and As_2S_3, the agreement is remarkably good. Although the low value of K_0 for As_2S_3 may imply the existence of additional scattering processes, the large value of K_0 for amorphous SiO_2 could mean that some additional heat transport mechanism is operative.

REFERENCES AND NOTES

1. W. A. Phillips, Ed., *Amorphous Solids: Low Temperature Properties* (Springer-Verlag, Berlin, 1981).
2. P. W. Anderson, B. I. Halperin, C. M. Varma, *Philos. Mag.* **25**, 1 (1972).
3. W. A. Phillips, *J. Low Temp. Phys.* **7**, 351 (1972).
4. M. P. Zaitlin and A. C. Anderson, *Phys. Rev. B* **12**, 4475 (1975).
5. R. C. Zeller and R. O. Pohl, *ibid.* **4**, 2029 (1971).
6. E. Akkermans and R. Maynard, *ibid.* **32**, 7850 (1985).
7. S. Alexander, O. Entin-Wohlman, R. Orbach, *ibid.* **34**, 2726 (1986).
8. J. E. Graebner, B. Golding, L. C. Allen, *ibid.*, p. 5696.
9. C. C. Yu and J. J. Freeman, *ibid.* **36**, 7620 (1987).
10. G. A. Slack, in *Solid State Physics*, F. Seitz and D. Turnbull, Eds. (Academic Press, New York, 1979), vol. 34, p. 1.
11. A. Einstein, *Ann. Phys. (N.Y.)* **35**, 679 (1911).
12. D. G. Cahill and R. O. Pohl, *Annu. Rev. Phys. Chem.* **39**, 93 (1988).
13. D. G. Cahill, thesis, Cornell University (1989).
14. _____ and R. O. Pohl, *Solid State Commun.* **70**, 927 (1989).
15. P. B. Allen and J. L. Feldman, *Phys. Rev. Lett.* **62**, 645 (1989).
16. D. Stauffer, *Introduction to Percolation Theory* (Taylor & Francis, Philadelphia, 1985), p. 17.
17. G. F. Weir and G. J. Morgan, *J. Phys. F* **11**, 1833 (1981).
18. Increasing amount of fluctuation from one configuration to the next is seen for $p \leq 0.5$.
19. The phonon dispersion relation on a simple cubic lattice with $p = 1$ is given by

$$\omega^2 = 4\beta(3 - \sum_{i=1}^{3} \cos k_i a_0)/m$$

where k_i, $i = 1$ to 3, denotes the wave vector in either the x, y, or z direction.
20. Q. J. Chu and Z. Q. Zhang, *Phys. Rev. B* **39**, 7120 (1989).
21. R. Haydock, in *Solid State Physics*, H. Ehrenreich, F. Seitz, D. Turnbull, Eds. (Academic Press, New York, 1980), p. 216.
22. D. G. Cahill and R. O. Pohl, *Phys. Rev. B* **35**, 4067 (1987).
23. No literature value could be found. Therefore, we have used the value similar to PMMA.
24. C. A. Condat and T. R. Kirkpatrick, in *Scattering and Localization of Classical Waves in Random Media*, P. Sheng, Ed. (World Scientific, Singapore, 1990), p. 423.
25. We acknowledge helpful discussions with Z. Q. Zhang and useful comments on the manuscript by R. O. Pohl.

18 March 1991; accepted 3 June 1991

Quantification of Primary Versus Secondary C–H Bond Cleavage in Alkane Activation: Propane on Pt

W. HENRY WEINBERG* AND YONG-KUI SUN†

The trapping-mediated dissociative chemisorption of three isotopes of propane (C_3H_8, $CH_3CD_2CH_3$, and C_3D_8) has been investigated on the Pt(110)-(1 × 2) surface, and both the apparent activation energies and the preexponential factors of the surface reaction rate coefficients have been measured. In addition, the probabilities of primary and secondary C–H bond cleavage for alkane activation on a surface were evaluated. The activation energy for primary C–H bond cleavage was 425 calories per mole greater than that of secondary C–H bond cleavage, and the two true activation energies that embody the single measured activation energy were determined for each of the three isotopes. Secondary C–H bond cleavage is also preferred on entropic grounds, and the magnitude of the effect was quantified.

BOTH DUE TO ITS EXTREME TECHNOLOGICAL importance and its intrinsic scientific challenge, the activation of alkane molecules by both homogeneous transition metal complexes (*1*) and heterogeneous surfaces (*2–4*) has been a very active area of research during the past decade. Alkane activation by transition metal surfaces (C–H bond cleavage resulting in dissociative chemisorption) has been studied by both molecular beam scattering (*5–8*) as well as "bulb" chemical reaction (*9–13*) investigations. Two fundamentally different reaction mechanisms have emerged from these studies of alkane activation. These two mechanisms are the following: (i) direct dissociation; and (ii) trapping-mediated dissociative chemisorption.

Direct dissociative chemisorption occurs on the time scale of a collision between the gas-phase molecule and the surface ($\lesssim 10^{-12}$ s), and the rate of this reaction depends primarily on the translational and internal energies of the gas-phase molecule (and to a lesser extent on the temperature of the surface) (*3*, *4*). In trapping-mediated dissociative chemisorption, the gas-phase molecule is trapped in the potential field of the surface (that is, it is adsorbed physically in the case of an alkane) and it accommodates to the temperature of the surface. The physically adsorbed molecule may then either desorb with a rate coefficient k_d (with an associated activation energy of desorption E_d) or it may react (dissociate) with a rate coefficient k_r [with an associated activation energy of reaction (E_r) (*4*, *14–17*)]. The rate of this reaction is a function of the surface temperature. The gas temperature is important only insofar as it affects the probability of trapping into the physically adsorbed state. When a molecular beam of reactants with sufficiently high translational energy impinges on a surface, the direct mechanism would be favored primarily because the trapping probability becomes very small in this case. In a bulb rather than a beam environment, which one encounters more typically in technological processes, the trapping-mediated mechanism is expected to dominate. An exception to this rule would occur if $E_r - E_d$ were sufficiently large that the surface temperature would have to be so high for the reaction to occur that the residence time of the molecular adsorbate is too short for accommodation and reaction through this trapping-mediated mechanism. This appears to be the case, for example, for the dissociative adsorption of methane on low-index surfaces of nickel (*3*, *6*, *11*), but it is not the case for methane on the Pt(110)-(1 × 2) surface (*13*). For all alkanes with the possible exception of methane, in a bulb experiment with a Maxwell-Boltzmann distribution of velocities, one expects the trapping-mediated mechanism to dominate.

The results of an investigation of the dissociative chemisorption of propane on the reconstructed and highly corrugated Pt(110)-(1 × 2) surface (*10*, *13*, *18*) are reported here, where the trapping-mediated mechanism of chemisorption occurs. Three different isotopes of propane (C_3H_8, C_3D_8, and $CH_3CD_2CH_3$) were used to determine the relative probability of primary (1°) versus secondary (2°) C–H bond cleavage in linear alkanes such as propane, in which there are two inequivalent kinds of C–H bonds. Since the bond dissociation energy of the 1° C–H bonds in propane is 97.9 ± 1 kcal/mol whereas that of the 2° C–H bonds is 95.1 ± 1 kcal/mol (*19*), and because it seems unlikely that the bond dissociation energies of the two platinum-propyls that are formed in the reaction would have a difference that is this great, one might expect a priori a preference for the formation of Pt–$CH(CH_3)_2$ (*17*). Steric constraints might also favor one reaction product over the other in a heretofore unknown way. This is an important issue which has rather profound mechanistic implications insofar as selectivity in heterogeneous catalysis is concerned. As discussed below, a propensity for the 2° C–H bond-cleavage reaction for propane on this surface of platinum has been confirmed and quantified.

The measurements were carried out in an ion-pumped ultrahigh vacuum (UHV) microreactor (base pressure of 3×10^{-10} torr, volume of 30 cm^3) (*13*, *20*). The experi-

Department of Chemical Engineering, University of California, Santa Barbara, Santa Barbara, CA 93106.

*To whom correspondence should be addressed.
†Present address: Department of Chemistry BG-10, University of Washington, Seattle, WA 98195.